Vol 18 No 8, August 2009
1674-1056/2009/18(08)/3473-11

Chinese Physics B

© 2009 Chin. Phys. Soc.
and IOP Publishing Ltd

Density and impurity profile behaviours in HL-2A tokamak with different gas fuelling methods*

Cui Zheng-Ying(崔正英)†, Zhou Yan(周 艳), Li Wei(李 伟),
Feng Bei-Bin(冯北滨), Sun Ping(孙 平), Dong Chun-Feng(董春凤),
Liu Yi(刘 仪), Hong Wen-Yu(洪文玉), Yang Qing-Wei(杨青巍),
Ding Xuan-Tong(丁玄同), and Duan Xu-Ru (段旭如)

Southwestern Institute of Physics, Chengdu 610041, *China*

(Received 8 November 2008; revised manuscript received 23 December 2008)

The electron density profile peaking and the impurity accumulation in the HL-2A tokamak plasma are observed when three kinds of fuelling methods are separately used at different fuelling particle locations. The density profile becomes more peaked when the line-averaged electron density approaches the Greenwald density limit $n_{\rm G}$ and, consequently, impurity accumulation is often observed. A linear increase regime in the density range $n_{\rm e} < 0.6n_{\rm G}$ and a saturation regime in $n_{\rm e} > 0.6n_{\rm G}$ are obtained. There is no significant difference in achieved density peaking factor $f_{\rm ne}$ between the supersonic molecular beam injection (SMBI) and gas puffing into the plasma main chamber. However, the achieved $f_{\rm ne}$ is relatively low, in particular, in the case of density below $0.7n_{\rm G}$, when the working gas is puffed into the divertor chamber. A discharge with a density as high as $1.2n_{\rm G}$, i.e. $n_{\rm e} = 1.2n_{\rm G}$, can be achieved by SMBI just after siliconization as a wall conditioning. The metallic impurities, such as iron and chromium, also increase remarkably when the impurity accumulation happens. The mechanism behind the density peaking and impurity accumulation is studied by investigating both the density peaking factor versus the effective collisionality and the radiation peaking versus density peaking.

Keywords: plasma radiation, impurity accumulation, density peaking
PACC: 5255, 5225

1. Introduction

Density profile peaking is favourable for the enhancement of plasma performance, such as improving plasma confinement by 30% compared with that in H-mode discharges with low density in ASDEX Upgrade,[1] increasing the bootstrap current fraction and the fusion power in burning plasma.[2] However, the peaked density profile usually causes impurity accumulation, which means that radial profiles of impurity density tend to be more peaked than the main ion density profile and, consequently, the degradation of the performance appears as an enhanced radiative power loss and a dilution of ions.[3–5] This phenomenon makes the further improvement on the background plasma confinement and the control of density more difficult, thereby becoming a severe problem under high recycling conditions. On the other hand, the peaked density profiles usually occur in tokamaks even when the fuelling is peripheral. Anomalous particle transport, such as the so-called anomalous particle pinch, is wisely discussed as a candidate for the particle distribution for the discharge with auxiliary heating when the classical and the neoclassical transport theories fail to adequately explain the experimental findings. Moreover, a natural and quasi-steady state particle transport barrier around $r/a = 0.6$–0.7 has recently been observed in the Ohmic plasma in HL-2A as a new observation of density distribution.[6] Therefore, it is important to characterize experimentally the plasma conditions which lead to density peaking and impurity accumulation, as well as to find a compatible condition under which a good plasma confinement with a tolerable impurity radiation in plasma core region could exist. In general, the density profile, together with the impurity profile, is strongly affected by many factors, such as additional heating methods (electron heating or ion heating) and fuelling methods (central fuelling or peripheral fuelling), from the experimental point of view. In order to study the effect of particle source on the particle distribution, we use only the Ohmic heating discharges with different

*Project supported partially by the National Natural Science Foundation of China (Grant No 10475022).
†Corresponding author. E-mail: cuizy@swip.ac.cn

fuelling methods.

In this paper the behaviours of density profile and impurity accumulation in a deuterium plasma of the HL-2A tokamak are investigated when three kinds of fuelling methods are separately used which have different fuelling particle locations. In Section 2 the main diagnostics involved in this study and the particles' penetration related to each fuelling method are described. Experimental results are presented and discussed in Section 3. The parametric dependences of the density peaking and impurity accumulation are discussed in Section 4 with a dataset assembled for this study. The final section is devoted to a summary and discussion.

2. Experimental setup and particle source location

the HL-2A tokamak is a large divertor tokamak, which can be operated in different poloidal divertor configurations. The geometrical parameters of the HL-2A tokamak are major radius $R = 165$ cm and minor radius $a = 40$ cm. Typically, it is operated at a toroidal magnetic field $B_t = 2.4$ T and a plasma current between 200 kA and 480 kA.[7,8] In the present study, the HL-2A tokamak is run in a low single null closed divertor configuration with a plasma current of about 180 kA and a toroidal magnetic field of around 1.4 T.

The main diagnostics involved in this study are eight-chord HCN laser interferometry ($\lambda = 0.337$ mm) to measure electron density in the central region of the plasma ($\rho = r/a < 0.6$, where ρ is the normalized poloidal flux coordinate) with a spatial resolution of $\sim$ 7 cm,[9] seven-chord Thomson scattering for electron temperature measurement with a spatial resolution of about 3 cm and a time resolution of about 100 ms, and a microwave reflectometer of 26.5 GHz–40 GHz also for electron density measurement, which covers a density range from 0.8 to 2.0$\times$ 10^{19} m^{-3}. The ion temperature measurement in the HL-2A tokamak plasma is a single line-of-sight charge exchange neutral particle analyzing system. The information about impurity profile can be obtained by a five-array of soft x-ray cameras with 20 line-of-sight in each array, which give a spatial resolution of 2.5 cm and a time resolution of 10 μs, equipped with 25 μm thick beryllium foils, and three-array bolometers with sixteen-chord in each array, which give the same spatial resolution as that of soft x-ray measurement and 50 μs for time resolution. The energies range from 1 keV to 10 keV for the soft x-ray cameras and from 1 eV to 10 keV for the bolometers. The characteristic emission lines from different impurity elements are measured by a normal incidence vacuum ultraviolet (VUV) spectrometer equipped with two concave gratings blazed at 80 nm and 150 nm and with a windowless back-illuminated charge coupled device (CCD) detector of 256 $\times$ 1024 pixels.[10] The effective plasma charge, $Z_{\rm eff}$, can be derived from the measurements of bremsstrahlung radiation which has 8 spatial channels.

A tangential D_α emission detective array (46 channels) is used to determine the fuelling particle deposition location. Two fast gauges located in the plasma main chamber and in the divertor chamber, separately, are also applied to neutral gas pressure measurement, which gives information about the fuelling source and the divertor pumping efficiency. Three kinds of fuelling methods, which are ordinary gas puffing from the plasma main camber (GPp) and from the high field side of the divertor chamber (GPd), and supersonic molecular beam injection (SMBI) from the low field side of the plasma chamber, are investigated in this study. In general, a deeper penetration can be achieved by SMBI and the location of the fuelling source usually reaches $\sim 0.7a$–$0.8a$ deep.[11] Intensity profiles of D_α at several different times are plotted in Fig.1 for the case of the SMBI. The solid lines with solid symbols represent the radial profiles of the neutral particles at the early phase when their density increases, while the dot lines with open symbols refer to the neutral particle profiles at the later phase when neutral particle density decreases.

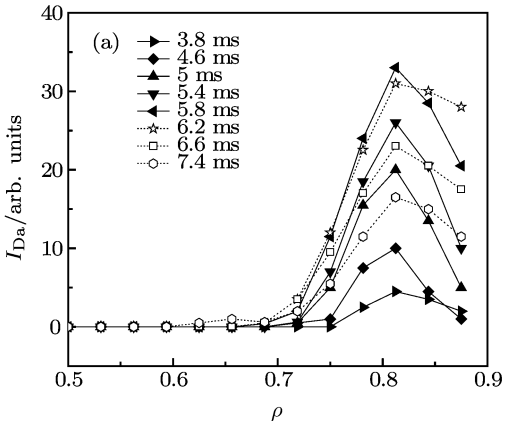


Fig.1. Spatial distributins of D_α intensities in the case of SMBT at several time moments.

It is clearly shown from Fig.1 that the peaks of

the D_α intensity are located in a range of ρ ($\rho = r/a$)=0.7–0.9 both in the increase phase and in the decrease phase. Therefore, the neutral particle source fuelled by SMBI mostly can penetrate into the last closed flux surface (LCFS), namely the separatrix. Some discharges even have deeper penetration of neutral particles: they can even arrive at the plasma centre as given in Ref.[12]. In contrast, the locations of the fuelling particle source both for GPp and for GPd, measured also by D_α emission, are only close to the separatrix from the outside region. In particular, the neutral gas for GPd must go through the divertor throat to reach the plasma main chamber and spread throughout the vacuum vessel. The initial position of neutral gas for the GPp is more likely to be restricted to the midplane of the machine since the valves are all located there. These features can obviously affect the efficiencies of gas puffing and divertor pumping, which will be discussed in Section 4.

3. Experimental results

A dramatic increase of plasma radiation in the plasma core is frequently observed in high density Ohmic discharges, where the electron density is usually close to or higher than the Greenwald density limit, in limiter and divertor configurations with the gas fuelling methods mentioned above in the HL-2A tokamak. The experimental results presented below will be divided into three parts according to the fuelling methods applied.

3.1. Gas puffing from the low field side of plasma chamber (GPp)

The measurements for a typical discharge with a normal gas puffing are given in Fig.2, showing the time evolutions of main plasma parameters (from top to bottom): (a) plasma current; (b) line-averaged electron densities from two interferometer channels: one passes horizontally through the centre at $\rho = 0.1$ and the other is close to the minor radius of plasma at $\rho = 0.6$; (c) soft x-ray emissions at centre and at $\rho = 0.4$; (d) the neutral gas pressures in the plasma main chamber, P_p, and in divertor chamber, P_d. The soft x-ray emission shown in Fig.2(c) increases sharply in a very central region and remains constant in the outer region of plasma when the modulated gas puff is turned off at $t = 750$ ms, which is indicated in the P_p signal in Fig.2(d). Meanwhile, the electron density of the central chord remains almost unchanged and the one at $\rho = 0.6$ slightly decreases, which is shown in Fig.2(b). Consequently, the density profile becomes peaked. The central electron temperature measured by Thomson scattering for this shot is not available, but in similar discharges, it does not show any significant change during the sharply increasing central radiation. Therefore, the dramatic increase of the central soft x-ray radiation should be a consequence of impurity accumulation rather than the increase of the central electron density or temperature. The neutral gas pressures in the plasma main chamber (P_p) and in the divertor chamber (P_d), given in Fig.2(d), do not show any clear change when the gas puffing is stopped. That means that the change of density profile is not directly caused by the increasing of influx of the neutral source at plasma edge, but a transient behaviour in plasma central region may occur.

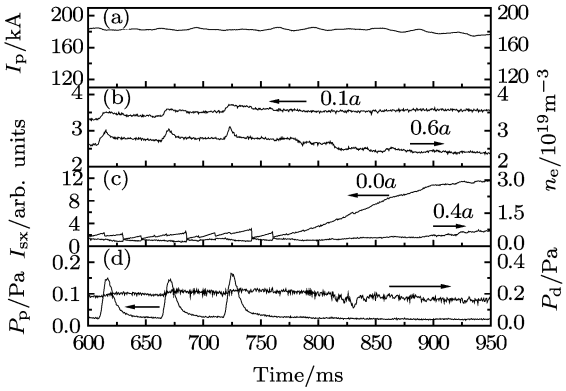


Fig.2. Temporal evolutions of plasma parameters (from top to bottom): (a) plasma current, (b) electron densities at $r = 0.1a$ and $0.6a$, (c) soft x-ray emissions at centre and at $r = 0.4a$, (d) neutral gas pressures in the plasma main chamber and in divertor chamber, P_p and P_d respectively.

The dramatic increase of radiation from bolometer measurement and the radial profiles of radiated power before and after the impurity accumulation are given in Figs.3(a) and 3(b) respectively. Figure 3(a) shows that the plasma radiations in the two central chords increase remarkably, typically, from ~ 0.8 arb. unit to 2.0 arb. unit for the central chord $r = 3.1$ cm, and the others in the outer region of plasma ($r >$ 15 cm) remain unchanged with time. The radiations along the chords at $r = 15$ cm and $r = 20.6$ cm even decrease slightly. That means that the gradient of radiation in the very central region ($r < 15$ cm) becomes steep in the final phase of this pulse. It can be further found from Fig.3(b) that there is a very much peaked radiation profile with the total increment of radiation by a factor of about 2.6 in the central region

($r < 15$ cm) at $t = 900$ ms compared with that at $t = 800$ ms.

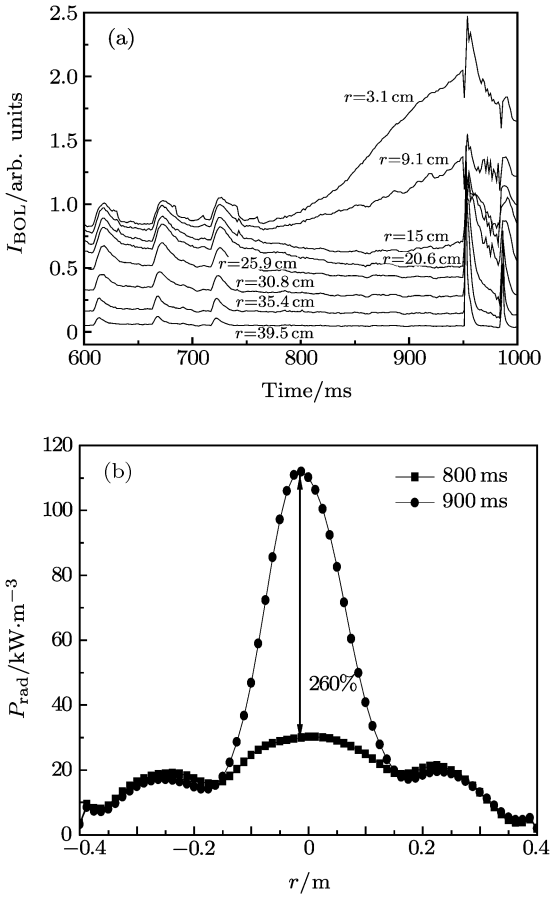


Fig.3. Time traces of line-integrated signals from bolometer for different chords (a) and the radial profiles of the radiation power at $t = 800$ ms and 900 ms (b).

The time traces of electron density profiles are depicted in Fig.4. The density peaking factor is defined as the ratio between the densities at $r = 0.1a$ and at $r = 0.6a$. It is noticed that the density profile remains broad and the peaking factor is around 1.5 in the time range below 800 ms. Then, the density profile becomes more peaked and the peaking factor is greater than 1.6 thereafter. This experimental result strongly suggests that the impurity accumulation is correlated with the peaking of density profile in plasma core.

Copper, iron and chromium are the most dominant metallic impurities in the present HL-2A plasma. The intensities of their characteristic emission lines in the VUV spectra used for analyzing the impurity content of the plasma are considerably increased when the central plasma radiation increases. An example is given in Fig.5, where the time-dependent CrXIV (389.81 Å) (1 Å=0.1 nm) and FeXVI (335.407 Å) line emissions from the same pulse mentioned above are plotted. Their ionization potentials are 384 eV and 489 eV, respectively. It is shown in Fig.5 that intensities of chromium and iron both strongly increase in a time range from 750 ms to 1000 ms. However, the intensities of low Z impurities, such as carbon and oxygen, generally do not change so much.

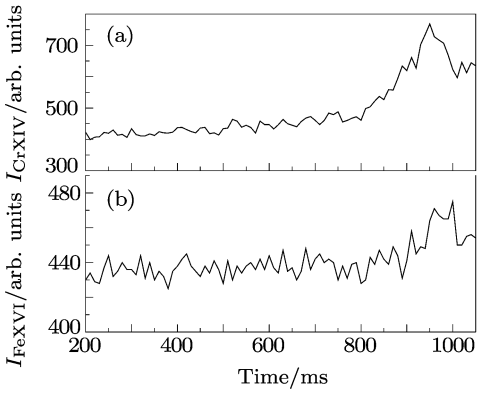


Fig.5. Line emissions of CrXIV (a) and FeXVI (b).

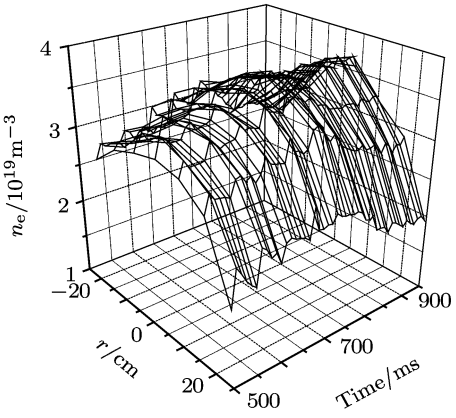


Fig.4. Temporal evolutions of density profile.

3.2. Supersonic molecular beam injection (SMBI)

Similar phenomena of impurity accumulation have been observed in the discharges with supersonic molecular beam injection (SMBI) when density profile becomes peaked enough. The density peaking factor and the line-integrated radiation from the bolometer in different chords are plotted in Figs.6(a) and 6(b), respectively, with plasma current $I_p = 180$ kA and electron density $n_e = 2.9 \times 10^{19}$ m^{-3} of pulse No. 7551. Note that the region ($r < 15$ cm), where the bolometric signals sharply increase when the density

peaking factor exceeds 1.6, is the same as that observed in the GPp case. The increment of radiation in this discharge is about a factor of 3.

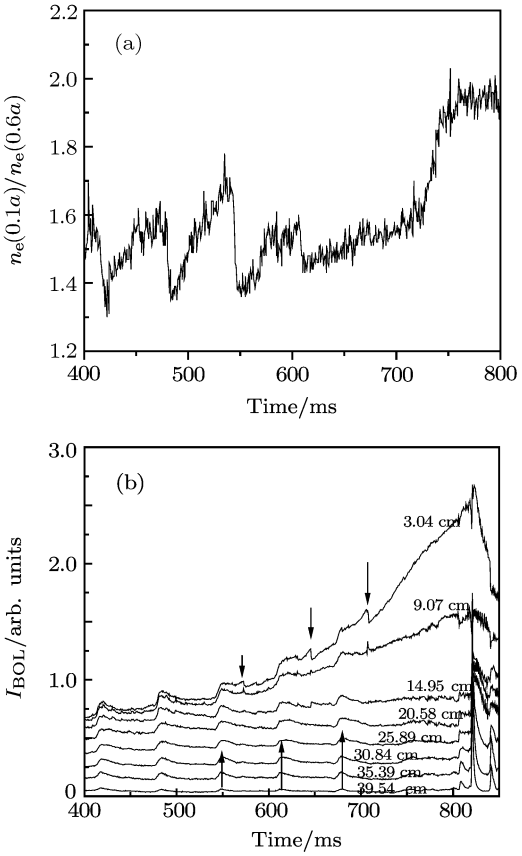


Fig.6. Temporal evolutions of density peaking factor (a) and bolometric signals in different chords (b).

It is worthwhile noting that the effect of sawtooth on impurity accumulation is also present in this discharge. There are three big sawteeth at $t = 572$ ms, 646 ms and 705 ms, marked by three vertical arrows pointing downwards in Fig.6(b). Meanwhile, there are three vertical arrows pointing upwards at 541 ms, 606 ms and 670 ms, indicating the moments when working gas pulses are injected by the SMBI. The increase of radiation is obvious, when the gas pulses are injected, with the increase of electron density. However, it is clearly shown that there is a sudden drop of radiation in the central chord during the sawtooth crash, while the intensities measured from the other chords do not show any observable decline. Furthermore, the increase of radiation in the core becomes very fast when the sawteeth have totally disappeared in the final stage of this shot. In general, strong and periodic sawtoothing events are experimentally confirmed and theoretically supported by stopping impurity accumulation in plasma with the great enhancement of the transport by the magnetic island where the degenerate magnetic flux surface allows particles to move radially by rapid parallel flow.[13] This phenomenon was also reported in an HL-2A tokamak experiment with the injection of impurities accompanied by the use of the laser blow-off method.[14]

3.3. Gas puffing from high field side of divertor chamber (GPd)

The impurity accumulation has also been observed in the discharge with gas puffing from the high field side of the divertor chamber (GPd) when the density profile becomes more peaked. The time evolutions of four-chord line-averaged density and of chord-integrated radiative signals from two bolometric chords, together with soft x-ray signals from several chords, are presented in Figs.7(a) and 7(b), respectively. The main plasma parameters for this pulse No. 7285 are nearly the same as those for the discharges mentioned above. The radiation intensities obtained from the bolometer and the soft x-ray signals show a significant increase in the same area, where half of the central plasma occupies ($r < 0.5a$), only when the gradient of density

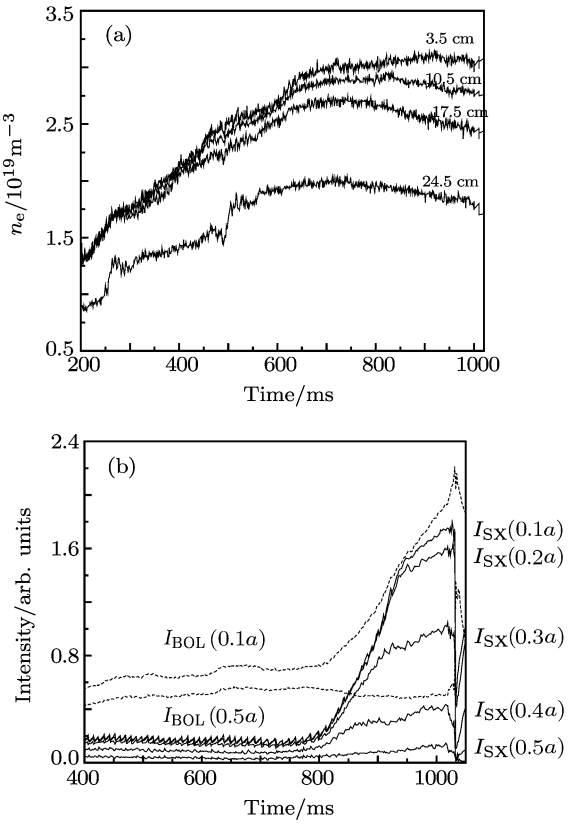


Fig.7. Temporal evolutions of line-averaged density in four chords (a) and line-integrated radiative from bolometer in two chords (dotted lines) and from soft x-ray in five chords (solid lines) (b).

increases in the time region above 800 ms with line-averaged density in the core being nearly unchanged. The intensities obtained both from the bolometer and from the soft x-ray signals beyond this region still remain constant. The increase of intensity in the core is very significant with the increase of radiation, or rather, a factor of ~ 3.3 larger than that at $t = 850$ ms.

The discharges discussed above just show that the radiation in the core does increase rapidly with the increase of density peaking factor. In fact, one also observes that the radiation remains constant at a relatively high level for a time scale longer than the energy confinement time if the density profile does not become more peaked. An example is given in Fig.8, where the line-integrated radiation from the bolometer in a time period and the density peaking factor are presented. It is shown that the central radiation gradually increases with density peaking factor $f_{\rm ne}$ increasing to about 1.5, i.e. $f_{\rm ne} \sim 1.5$, at $t = 600$ ms. Thereafter, $f_{\rm ne}$ shows a slight decline but no further increase. In contradiction to the previous observation, the central radiation keeps increasing in just a short time period, and then holds constant for about 100 ms until the end of this pulse where $f_{\rm ne}$ reduces to about 1.3. The value of 1.5 for $f_{\rm ne}$ in this pulse looks like a typical value to trigger the impurity accumulation, which will be discussed in the next section. The results also show a possibility to actively control the impurity accumulation by controlling the density profile.

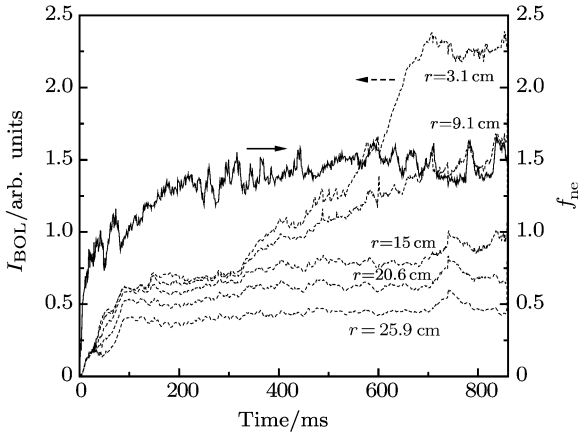


Fig.8. Time evolutions of line-integrated radiations from bolometer in several chords (dotted lines) and density peaking factor (solid line).

The effect of magnetic configuration on impurity accumulation is also investigated. Two typical discharges with identical main plasma parameters are shown in Fig.9, where pulse No. 6840 is for a discharge with a limiter configuration while pulse No. 7291 is for a discharge with a divertor configuration. The traces of line-averaged electron density and plasma radiation power (Figs.9(a) and 9(d)), bolometric signals at $r = 0.5a$ and $r = 0.1a$ (Figs.9(b) 9(e)), soft x-ray signals at $r = 0.5a$ and $r = 0.1a$ (Figs.9(c) and 9(f)) are given for both pulses, respectively. The increases of the core radiation, which are demonstrated by the signals of $I_{\rm BOL}$ $(0.1a)$ and $I_{\rm SX}$ $(0.1a)$, are significant when the density peaking factor is larger than 1.8 for pulse No. 6840 and 1.5 for pulse No. 7291. However, the radiations obtained from bolometry and from soft x-ray signals at $r = 0.5a$ for pulse No. 6840 with limiter configuration (Figs. 9(b) and 9(c)) are too much higher than those for pulse No. 7291 with divertor configuration ((Figs.9(e) and 9(f)), respectively. Moreover, the total plasma radiation power shows a pronounced increase in the limiter case (Fig.9(a)) and remains nearly

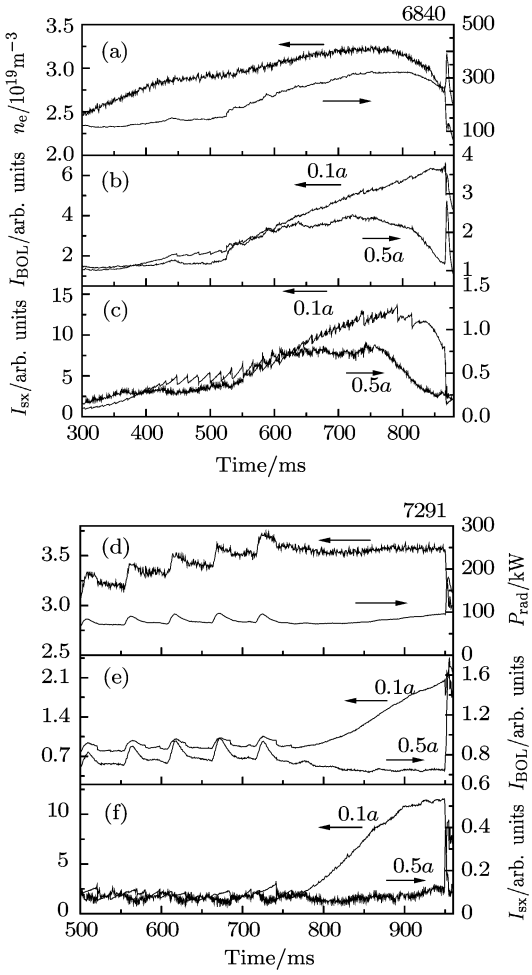


Fig.9. Time traces of line-averaged electron densities and plasma radiation powers (a, d), bolometric signals at $r = 0.5a$ and at $r = 0.1a$ (b, e), soft x-ray signals at $r = 0.5a$ and at $r = 0.1a$ (c, f) in two discharges: 6840 for limiter configuration and 7291 for divertor configuration.

constant for the divertor case (Fig.9(d)). That means that the impurity accumulation for the limiter case seems to be the consequence of total impurity content increasing through the strong plasma-wall interaction. This result is consistent with the conclusion that impurity content can be dramatically reduced in the divertor configuration compared with that in the limiter configuration.[7] The ratio of volume integrated radiation power $P_{\rm rad}$ to input power $P_{\rm in}$ remains relatively low ($P_{\rm rad}/P_{\rm in} \sim 0.5$) for the divertor case. Therefore, this observation also confirms that the change of the radiation in the very central region is not due to the variation in the impurity source strength but is purely an effect of modified core transport.[15]

4. Parametric dependence analysis

4.1. Description of the Ohmic data set

A data set covering the usual parameter range ($150 < I_{\rm p} < 190$ kA, $1.3 < B_{\rm t} < 1.5$ T, $0.6 < n_{\rm e} < 5 \times 10^{19}$ m^{-3}, $0.2 < n_{\rm e}/n_{\rm G} < 1.2$, $P_{\rm heat} < 0.5$ MW) is assembled to investigate the parametric dependence of the density peaking and impurity accumulation, with three gas fuelling methods used separately, in a whole experimentally accessible density region during the 2007 experimental campaign. $n_{\rm G}$ is the Greenwald density limit and $P_{\rm heat}$ is the input power. About 124 Ohmic discharges are included in this dataset with about 48 observations for GPp, 52 for SMBI and 24 for GPd. The safety factor profiles in all discharges presented in this study are monotonic, with the value of safety factor at the plasma boundary being in a range of 2.5–5.

The definition of density peaking factor, which is given in Subsection 3.1, is considered to be more accurate than the generally used definition of $n_{\rm e}(0)/\langle n_{\rm e}\rangle$ for the description of the shape of density profile, and the present definition may reduce the error bars caused by the solution of the Abel inversion problem because the available channels of the HCN interferometer are limited to 7 chords in the 2007 campaign on the HL-2A tokamak. In order to characterize the radiation profile, the peaking factor of radiation, $f_{\rm rad}$, is also simply defined as the ratio of bolometric signal at $r = 0.1a$ to that at $r = 0.5a$, which is similar to the definition of the density peaking factor of $f_{\rm ne} = n_{\rm e}(0.1a)/(0.6a)$.

4.2. Characteristics of the density profile peaking

Figure 10 shows the electron density peaking factor $f_{\rm ne}$ as a function of the normalized density to the Greenwald density limit $n_{\rm e}/n_{\rm G}$ for GPd (stars), GPp (triangles), and SMBI (squares). The open (Fig.10(a)) and solid (Fig.10(b)) symbols denote plasmas without and with disruptions, respectively.

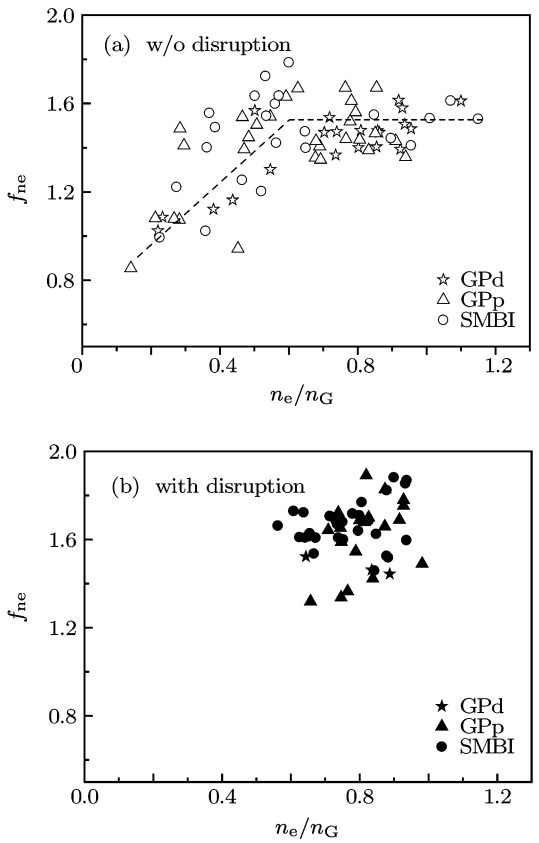


Fig.10. Curves for density peaking factor versus Greenwald fraction (a) without disruption and (b) with disruption, where stars, triangles, and squares represent the cases of fuelling with GPd, GPp, and SMBI respectively.

Note that density peaking increases with the increase of Greenwald fraction, $n_{\rm e}/n_{\rm G}$, in a density range of $n_{\rm e} < 0.6n_{\rm G}$ and shows a saturated tendency at $n_{\rm e} > 0.6n_{\rm G}$, which is clearly shown by a dashed line in Fig.10(a). This feature is similar to the observations in the plasma energy confinement with the so-called linear Ohmic confinement regime (LOC) and saturated Ohmic confinement regime (SOC).[16] In general, the saturation of the energy confinement time $\tau_{\rm E}$ ($n_{\rm e}$) dependence is pronounced at $n_{\rm e} > 0.6n_{\rm G}$ and the confinement saturation is accompanied by an increase in density gradient in the core region. The change of density profile in the core plays an important role in

the saturation of confinement and impurity accumulation.

Also, it is indicated in Fig.10(b) that disruptive discharges usually have higher $f_{\rm ne}$ and higher $n_{\rm e}$ where the densities are in a range of 0.6–1.0 $n_{\rm G}$. Some discharges without disruption in the high density regime ($n_{\rm e} > n_{\rm G}$) are achieved by SMBI and by GPd just after siliconization as a wall conditioning. However, the values of density peaking factor $f_{\rm ne}$ for these shots are all below 1.6. Moreover, no significant difference in the value of $f_{\rm ne}$ between SMBI and GPp is observed in the whole density range achieved, even though the penetration length of the neutral gas for SMBI is around 10 cm inside the LCFS. That means that the edge fuelling source as well as the presented deeper fuelling cannot be responsible for the density gradient in the plasma bulk, and implies the presence of inward particle convection. On the other hand, when the gas valve is in the divertor chamber a somewhat low $f_{\rm ne}$ is achieved compared with that in the discharge fuelled by SMBI and GPp, in particular, in the discharges with densities below $\sim 0.7 n_{\rm G}$. The difference in $f_{\rm ne}$ is perhaps due to the different edge neutral fluxes, which will be discussed below, rather than the change in particle transport.

In order to further study the phenomenon of density profile peaking, a dependence of $f_{\rm ne}$ on the collisionality, which is an essential ingredient in describing the electron dynamics, is investigated. Figure 11 shows that the value of $f_{\rm ne}$ increases with the increase of effective collisionality $\nu_{\rm eff} = 0.1 \cdot R \cdot Z_{\rm eff} n_{\rm e}/T_{\rm e}^2$,[17] where $n_{\rm e}$ and $T_{\rm e}$ are the electron density and the temperature, respectively, $Z_{\rm eff}$ the effective plasma charge and R the major radius of plasma column. The scattering of the data is mostly caused by the electron temperature measurement. However, the dependence of the density peaking factor on effective collisionality still explicitly shows a tendency to increase with the increase of density when $n_{\rm e}$ is lower than $0.6 n_{\rm G}$, and a saturated tendency when $n_{\rm e}$ is greater than $0.6 n_{\rm G}$. This result obtained from the Ohmic plasma with electron heating is consistent with the measurements from T-10 and FTU for the L-mode plasma[18] but contrary to the measurements from JET and AUG H-mode plasma with dominant ion heating where density peaking is found to decrease with increasing collisionality.[19,20] In the framework of the theory of ion temperature gradient (ITG) and trapped electron modes (TEMs), the tendency of density peaking to increase could be explained as a consequence of increasing anomalous particle pinch due to the partial TEM suppression when particles go towards higher collisionalities.[17−19] However, the stability of the drift turbulence used to interpret the experimental results is more complicated, which is beyond the scope of the present paper. Nevertheless, the experimental results presented here may offer some speculative considerations about the particle transport based on the turbulent plasma.

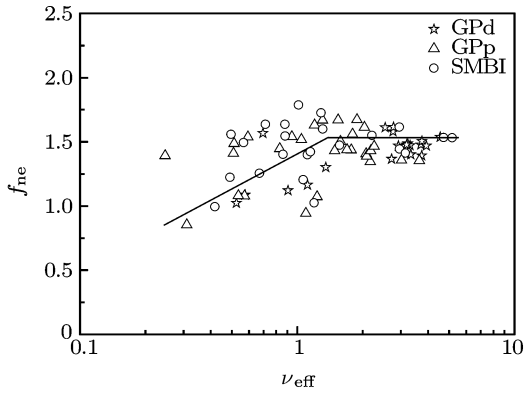


Fig.11. Density peaking factors versus effective collisionality, with three different fuelling methods used.

4.3. Characteristics of impurity accumulation

In order to study the parametric dependence of radiation profile on plasma condition, a peaking factor of radiation is plotted as a function of Greenwald fraction and density peaking factor in Figs.12(a) and 12(b), respectively. In Fig.12(a) $f_{\rm rad}$ does not clearly show any dependence on $n_{\rm e}/n_{\rm G}$. That means that the impurity profile peaking cannot be explicitly depicted by the line-averaged density. This figure does not indicate any clear difference in the dependence of $f_{\rm rad}$ on $n_{\rm e}/n_{\rm e}$ among these three kinds of gas fulling methods, in particular, the difference in discharge between the cases of GPd and GPp or SMBI. However, a clear relationship between $f_{\rm rad}$ and $f_{\rm ne}$ is shown in Fig.12(b). Note that for discharges with increasing density peaking, a tendency of increasing radiation profile peaking is observed. When $f_{\rm ne}$ is greater than ~ 1.4 most discharges are disruptive and the value of $f_{\rm rad}$ is also greater than 2. The value of $f_{\rm ne} = 1.4$ seems to be a typical value for the discharges which have more peaked radiation profiles. It is also shown in this figure that the $f_{\rm rad}$ values for the discharges without disruption are mostly less than 2 ($f_{\rm ne} < 2$) but large for the discharges with disruption ($f_{\rm rad} > 2$),

and they are obviously low for the discharges fuelled by GPd ($f_{ne} < 1.6$). All the data presented in this study show that the ratio of volume integrated radiation (P_{rad}) to the input power (P_{in}) remains relatively low when the density is close to the limit, in a range of 20%–60%. This could be interpreted as the fact that the change of the radiation from the very central region is not due to the changes in impurity source strength but it is purely a consequence of modified core transport. Moreover, there is no significant difference between the results obtained in the cases of SMBI and GPp. The experimental results presented here clearly show that the impurity accumulation is explicitly correlated with the parameter of the density peaking factor rather than the parameter of the Greenwald fraction, and the presented fuelling sources do not cause any significant difference between density peaking and impurity accumulation except for the one fueled in the divertor chamber.

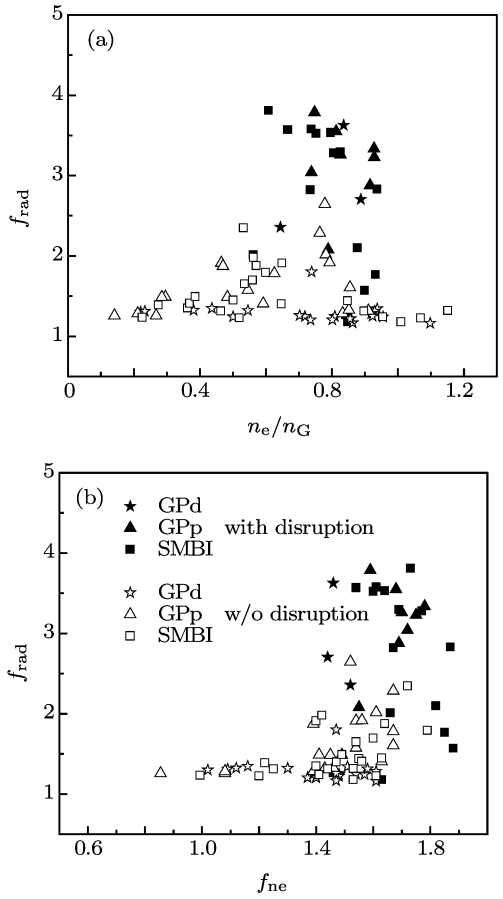


Fig.12. Radiation peaking factors as a function of Greenwald fraction (a) and density peaking factor (b). Open symbols represents the discharges without disruption; solid symbols refer to discharges with disruption; Stars, triangles and squares denote the cases fuelling with GPd, GPp and SMBI respectively.

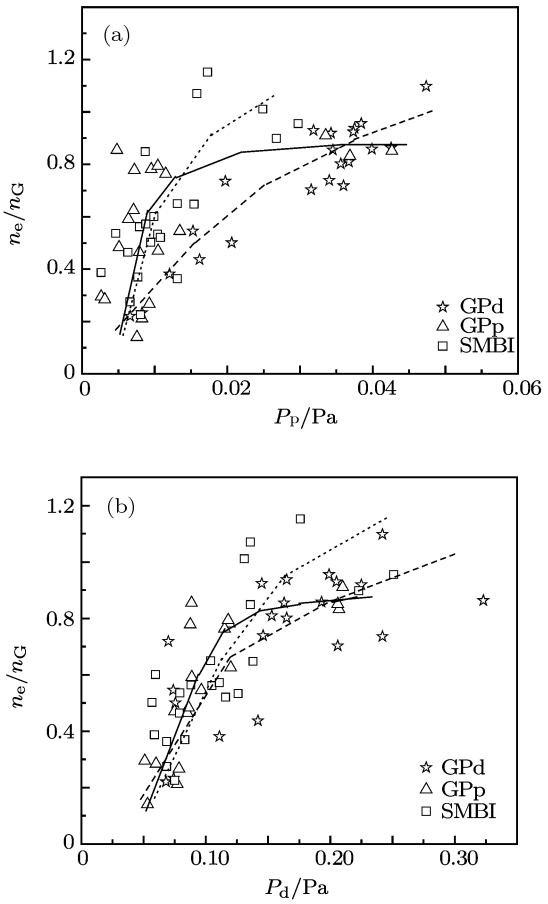


Fig.13. Curves for normalized n_e with Greenwald density limit as a function of neutral particle pressure in plasma main chamber P_p (a) and that in divertor chamber P_d (b), with three different fuelling methods used.

Typically in experiments, neutral flux density is measured by using the expression, $\Gamma_{mol} = 1/8 n_H \cdot c_H$, where n_H is the neutral density and c_H is the mean thermal speed of atoms based on the wall temperature. Therefore, the efficiencies of gas puffing and of divertor pumping can be investigated with the neutral gas pressures in the plasma main chamber (P_p) and in the divertor chamber (P_d), respectively, which are shown in Fig.13. The Greenwald fractions are plotted as a function of neutral particle pressure in the plasma main chamber (P_a) and in the divertor (P_d) in Figs.13(a) and 13(b), respectively. The symbols have the same meanings as those mentioned above. The dotted line shows the tendency of n_e/n_G versus P_p or P_d for SMBI, and the solid line for GPp and the dashed line for GPd. Clearly shown in Figs.13(a) and 13(b) are the differences in the relationship of n_e/n_G among the fuelling methods and in neutral pressure between in the plasma chamber and in the divertor chamber. When density is low (less than $0.8 n_G$), density increases quickly with the increase of neutral gas pressure in

the plasma main chamber for each fuelling method. However, when density is greater than $0.8n_{\rm G}$ electron density quickly becomes saturated with the further increase of neutral gas pressure for the normal gas fuelling method. It is saturated at $n_{\rm e} = 0.8n_{\rm G}$–$0.9n_{\rm G}$. This saturation leads the highest density achieved by GPp not to exceed $n_{\rm G}$ as shown in Fig.12(a). Meanwhile, the density can continually increase by increasing the neutral gas pressure for other two fuelling methods (SMBI and GPd). It is also observable that the neutral gas pressure needed to achieve the same density is a factor of ~ 1.7 for GPd and for GPp higher than that for SMBI when $n_{\rm e}/n_{\rm G} = 0.9$. This suggests that SMBI has a higher fuelling efficiency than GPd and GPp.

The divertor pumping efficiency is given in Fig.13(b). There is no significant difference among these fuelling methods when $n_{\rm e}/n_{\rm G}$ is less than 0.8. This result together with a much higher neutral gas pressure in the plasma main chamber for GPd can lead to a broad density profile. This may offer an interpretation of the discharges fuelled by GPd having low $f_{\rm ne}$.

5. Summary and discussion

Density peaking and impurity accumulation both can be observed in the discharges fuelled with three kinds of particle fuelling methods in the HL-2A tokamak. The parametric dependences of the density peaking and impurity accumulation are investigated with an experimental dataset assembled for this study with about 124 time slices. The experimental results clearly show that the density peaking factor increases with the increase of Greenwald fraction for the density range $n_{\rm e} < 0.6n_{\rm G}$ and saturates at $n_{\rm e} > 0.6n_{\rm G}$. The density value at the breaking-point $n_{\rm c} = 0.6n_{\rm G}$ is consistent with that observed in the plasma energy confinement with LOC and SOC regimes. No significant difference in $f_{\rm ne}$ between SMBI and GPp is observed, even though the penetration length of the neutral gas for SMBI is about 10 cm inside the LCFS. On the other hand, the achieved $f_{\rm ne}$ for GPd is relatively low, in particular, for the density below $\sim 0.7n_{\rm G}$. The difference is mainly due to the different higher neutral gas pressures in the plasma main chamber for using the GPd to achieve the same electron density as those achieved by using SMBI and GPp, while the divertor pumping efficiencies are kept similar for the three particle fuelling methods. This feature of GPd leads to a broad density profile compared with those in the cases of SMBI and GPp.

Impurity accumulation is often observed when the electron density peaking factor increases to a typical value of 1.4 and is explicitly correlated with the parameter of density peaking factor rather than the parameter of Greenwald fraction. The ratio of volume-integrated radiation $P_{\rm rad}$ to the input power $P_{\rm in}$ remains relatively low (in a range of 20%–60%). That means that the change of the radiation in the very central region is not mainly due to the change in impurity source strength but is purely caused by the modification of core transport. Some discharges without disruption in the high density regime ($n_{\rm e} > n_{\rm G}$) can be achieved by SMBI and by GPd with low $f_{\rm ne}$ (< 1.6) just after siliconization as a wall conditioning. Moreover, metallic impurities, such as iron and chromium, mostly contribute to the increase of radiation in the core.

A tendency of increase in density peaking factor versus effective collisionality is found which may provide an insight into the mechanism of the density peaking. As is known, the following factors can cause the density gradient in the core to increase: a change in particle source, an increase in anomalous particle and an increase in neoclassical particle pinch. The experimental result presented here shows that the particle source with a penetration of about more than 10 cm inside LCFS does not obviously affect the density gradient. The density peaking increases with effective collisionality increasing, which suggests that the anomalous particle pinch is increased by suppressing the trapped electron mode (TEM) in the high collisionality. The existence of anomalous transport in the HL-2A tokamak was reported in Refs.[8] and [14]. However, the neoclassical prediction sometimes can still be used to qualitatively understand the impurity transport related to the density peaking,[21] where the inward/outward pinch is driven by the temperature and density gradients. In this case, the ratio of convective speed to the diffusion coefficient V/D, the so-called peaking factor, is determined by the inverse of the density gradient length $Ln = n_{\rm e}/\nabla n_{\rm e}$. Therefore, the increase of the density gradient can drive an inward flux for the impurity accumulation. Whether the experiment can be fairly well interpreted with neoclassical theory alone, or with the neoclassical theory and an anomalous particle pinch combined together,

cannot be determined without the quantitative calculations of the density profile and the impurity distribution with using an appropriate model. Furthermore, the deeper fuelling sources, such as the pellet injection or neutral beam injection into the centre region of plasma, are needed to investigate the effect of particle source on density gradients. This work will be further done in a coming experimental campaign on the HL-2A tokamak.

Acknowledgment

The authors would like to thank all members of HL-2A experimental group, especially professors Cao Z, Liu Z T, Pan Y D and Fu B Z, Si P L, Lu J, Lu P, Zhang W and Cui C H for their help with the experimental operation. One of the authors (Cui Z) would like to thank professor Morita S and Dr. Guirlet R for their very valuable suggestions and discussions during the 35$^{\text{th}}$ EPS Plasma Physics Conference. The study was partially supported by the JSPS-CAS Core University Program in the Field of Plasma and Nuclear Fusion.

References

[1] Ryter F, Stober J, Stabler A, Tardini G, Fahrbach H U, Fruber O, Herrmann A, Kallenbach A, Kaufmann M, Kurzan A, Leuterer F, Maraschek M, Meister H, Peeters A G, Pereverzev G, Sips A C C, Suttrop W, Treutterer W, Zohm H and ASDEX Upgrade Team 2001 *Nucl. Fusion* **41** 537

[2] Progress in the ITER Physics Basis 2007 *Nucl. Fusion* **47** S18

[3] Angioni C, Peeters A G, Garbet X, Manini A, Ryter F and ASDEX Upgrade Team 2004 *Nucl. Fusion* **44** 827

[4] Dux R, Neu R, Peeters A G, Pereverzev G, Muck A, Ryter F, Stober J and ASDEX Upgrade Team 2003 *Plasma Phys. Control. Fusion* **45** 1815

[5] Jiao Y M, Zhou Y, Deng Z C, Ding X T, Liu Y and Wang E Y 2005 *Chin. Phys.* **14** 1600

[6] Xiao W W, Zou X L, Ding X T, Yao L H, Feng B B, Song X M, Zhou Y, Sun H J, Gao Y D, Yan L W, Yang Q W, Liu Yi, Dong J Q, Duan X R, Liu Yong, Pan C H and HL-2A Team 2008 *35*$^{\text{th}}$ *EPS Conf. on Plasma Physics* D5.003

[7] Cui Z Y, Sun, Pan Y D, Li W, Wang Q M, Cao Z and Wang M X 2006 *Chin. Phys.* **15** 0585

[8] Chen W, Cui Z Y, Sun P, Huang Y, Zhang P, Deng W, Pan Y D, Shi Z B, Zhou Y, Zheng Y Z and Yang Q W 2007 *Chin. Phys.* **16** 3451

[9] Zhou Y, Deng Z C, Liu Z T, Yi J, Tang Y W, Gao B Y, Tian C L, Li Y G and Ding X T 2007 *Rev. Sci. Instrum.* **78** 113503

[10] Cui Z Y, Sun P, Dong J F. Huang Y, Wang Q M, Fu B Z, Lu J, Chen W, Duan X R, Ding X T, Yang Q W and Morita S 2008 *Plasma Sci. Technol.* **10** 298

[11] Feng B B, Yao L Y, Li W, Chen C Y and Feng Z 2008 *Nucl. Fusion Plasma Phys.* **28** 97 (in Chinese)

[12] Yao L, Feng B, Chen C, Shi Z, Yuan B, Zhou Y, Duan X, Sun H, Lu J, Jiao Y, Ni G, Lu H, Xiao W, Li W, Pan Y, Hong W, Ran H, Ding X and Liu Yong 2007 *Nucl. Fusion* **47** 1399

[13] Nave M F F, Rapp J, Bolzonella T, Dux R, Mantsinen M J, Budny R, Dumortier P, Hellermann M von, Jachmich S, Koslowski H R, Maddison G, Messiaen A, Monier-Garbet P, Ongena J, Puratti M E, Strachan J, Telesca G, Unterberg B, Valisa M and Vries P de 2003 *Nucl. Fusion* **43** 1204

[14] Cui Z Y, Huang Y, Sun P, Zheng Y Z, Si P L, Lu J, Fu B Z, Zhang P, Pan Y D, Dong Y B, Deng W , Yang Q W and Ding X T 2006 *Chin. Phys. Lett.* **23** 2143

[15] Greenwald M 2002 *Plasma Phys. Control. Fusion* **44** R27

[16] Dong C F, Cui Z Y, Ji X Q, Zhou H Y, Feng B B, Sun H J, Li Y G and Yang Q W 2009 *Plasma Sci. Technol.* **11** 23

[17] Argioni C, Peeters G, Pereverzev G V, Ryter F and Tardini G 2003 *Phys. Plasmas* **10** 3225

[18] Kirneva N A, Gubarev I V , Kislov D A and Trukhina E V 2008 *Plasma Phys. Control. Fusion* **50** 06504

[19] Angioni C, Peeters A G, Pereverzev G V, Ryter F and Tardini G 2003 *Phys. Rev. Lett.* **90** 205003

[20] Weisen H, Zabolotsky A, Angioni1 A, FurnoI, Garbet X, Giroud C, Leggate H, Mantica P, Mazon D, Weiland J, Zabeo L and Zastrow K D 2005 *Nucl. Fusion* **45** L1

[21] Dux, R, Peeters A G, Gude A, Kallenbach A and Neu R 1999 *Nucl. Fusion* **39** 1509